Neptune's Dynamic Atmosphere from Kepler K2 Observations: Implications for Brown Dwarf Light Curve Analyses

Amy A. Simon[1], Jason F. Rowe[2], Patrick Gaulme[3], Heidi B. Hammel[4], Sarah L. Casewell[5], Jonathan J. Fortney[6], John Gizis[7], Jack J. Lissauer[8], Raul Morales-Juberias[9], Glenn S. Orton[10], Michael H. Wong[11], Mark S. Marley[8]

1. NASA Goddard Space Flight Center, Solar System Exploration Division (690.0), 8800 Greenbelt Road, Greenbelt, MD 20771, USA. Email: amy.simon@nasa.gov

2. Université de Montréal, Département de Physique, 2900 Boul. Édouard-Montpetit, Montréal, QC, Canada, H3T 1J4

3. New Mexico State University, Department of Astronomy, PO Box 30001, Las Cruces, NM 88003-4500, USA

4. AURA, Inc., 1212 New York Avenue NW, Washington, DC 20005, USA

5. University of Leicester, Department of Physics and Astronomy, University Road, Leicester, LE1 7RH, UK

6. University of California, Santa Cruz, Department of Astronomy & Astrophysics, 1156 High Street, 275 Interdisciplinary Sciences Building, Santa Cruz, CA 95064, USA

7. University of Delaware, Department of Physics and Astronomy, 104 The Green, Newark, DE 19716, USA

8. NASA Ames Research Center, Space Sciences & Astrobiology Division, MS 245-3, Moffett Field, CA 94035, USA

9. New Mexico Institute of Mining and Technology, Physics Department, Workman Center 345, 801 Leroy Place, Socorro, NM 87801, USA

10. Jet Propulsion Laboratory/California Institute of Technology, M/S 183-501, 4800 Oak Grove Drive, Pasadena, CA 91109, USA

11. University of California at Berkeley, Astronomy Department, Berkeley, CA 947200-3411, USA

Submitted to: *Astrophysical Journal*
Submitted: 29 October 2015
Figures: 8
Tables: 1
Supplemental online: 1 movie

Abstract

Observations of Neptune with the Kepler Space Telescope yield a 49-day light curve with 98% coverage at a 1-minute cadence. A significant signature in the light curve comes from discrete cloud features. We compare results extracted from the light curve data with contemporaneous disk-resolved imaging of Neptune from the Keck 10-meter and Hubble Space Telescope. The direct comparison validates the zonal wind profile and cloud feature variability information extracted from the light curve. Neptune's clouds vary in location and intensity on short and long time scales, with large discrete storms dominating the light curves; smaller or fainter clouds contribute to its variability. This has implications for the interpretation of information extracted from light curves of directly imaged exoplanets and cloudy brown dwarfs.

Keywords: planets and satellites: atmospheres (Neptune); planets and satellites: gaseous planets (Neptune); (stars:) brown dwarfs; stars: oscillations; stars: rotation; (stars:) starspots

1. Introduction

Brown dwarfs are substellar objects with masses below about 75 Jupiter masses, i.e., objects that cannot sustain hydrogen fusion (Chabrier et al. 2000). Brown dwarfs share many aspects with giant planets; both classes are predominantly composed of hydrogen and helium with an admixture of other elements; both have cool (at least by stellar standards) atmospheres; both have atmospheres with molecules and condensates that strongly influence the transport of energy by radiation. Review articles by Marley et al. (2013) and Burrows et al. (2001) compare and contrast the atmospheres of brown dwarfs and giant planets in more detail.

Many have searched for rotational and dynamical variability in brown dwarfs, dating back to shortly after their discovery (e.g., Tinney and Tolley 1999, Bailer-Jones and Mundt 2001, Gelino et al. 2002). Recent studies reveal photometric variability of many brown dwarfs in the mid infrared with the Spitzer Space Telescope (e.g., Metchev et al. 2015) and near-infrared spectral variability the Hubble Space Telescope (e.g., Apai et al. 2013, Yang et al. 2015). The most extensive ground-based survey was by Radigan et al. (2014), who found that L-type to T-type transition brown dwarfs are both more likely to be variable and show higher variability amplitudes than earlier and later spectral type objects.

Radigan et al. (2014) reviewed the long history of variability searches in a variety of spectral bandpasses with a multitude of time baselines and sensitivities. Despite the diversity in these searches, the unmistakable conclusion is that brown dwarfs are often variable. Amplitudes ranged from a typical few percent to the current record of 26% variation in J band over about 8 hours by the T1.5 dwarf 2MASS J21392676+0220226 (Radigan et al. 2012). This variability is typically attributed to inhomogeneous cloud cover resulting in a periodic brightness variation as the brown dwarf rotates.

A similar phenomenon of rotational modulation is seen for giant planets in our own solar system, extending back over a hundred years to visual reports of planetary brightness modulations (e.g., Cassini 1665). Ironically, for the larger giants, Jupiter and Saturn, "disk-resolved" measurements are extremely challenging because these objects are resolved by even small telescopes. For these reasons it has been difficult to place the abundant brown dwarf variability data in the context of giant planet variability. Gelino and Marley (2000) computed artificial visible and mid-infrared light curves for Jupiter by combining multiple full disk images, mapping them onto a sphere, and computing the expected rotational modulation in brightness. Rotational modulation was maximized at IR wavelengths due to maximum contrast for large storms, like the Great Red Spot, suggesting that similar results would hold for brown dwarfs with patchy clouds (Karalidi et al. 2015).

To help fill this gap in light curve measurement of giant planets, our collaboration observed Neptune with the repurposed Kepler Space Telescope as part of the K2 extended mission (Howell et al. 2014). We chose Neptune because it is bright

enough to extract a light curve with good photon statistics, but not so oversaturated for excess bleeding to substantially damage Kepler photometry. In addition, it has exhibited clear rotational modulation in the past (e.g., Joyce et al. 1977, Lockwood et al. 1991). Another key result from the Kepler prime mission was statistics of the size distribution of exoplanets, finding that hundreds were Neptune-sized (e.g., Batalha 2014). Thus, these observations provide ground truth for future photometry of exo-Neptunes (e.g., by space coronographs) and directly imaged exoplanets, in general, as well as brown dwarfs.

Kepler observations of Neptune were acquired from November 15, 2014 to January 18, 2015. Neptune and its large moon Triton were visible with 98% coverage and a 1-minute observation cadence starting December 1, 2015. From this high cadence data set, we generate a high-precision light curve over a 49-day period. Kepler observes over visible wavelengths (e.g., Rowe et al. 2009, Koch et al. 2010) from ~430 to 890 nm, and thus the light curve represents variations in Neptune's reflected solar flux, which necessarily combines variations both in Neptune's reflectivity and in the Sun itself. Neptune, however, is a resolved object in ground and space-based facilities. Thus, any inferred measurements from the light curves can be directly compared with known cloud features in the atmosphere, effectively providing ground truth for the Kepler light curve inferences.

In this paper, we described the results pertaining to Neptune's atmosphere, which dominates the Kepler light curve. Separate papers will address the photometric signal from the Sun and the signal from Neptune's interior. We show correlation of the Kepler light curve output with contemporaneous Keck and Hubble Space Telescope imaging data and compare with 20 years of Neptune cloud observations. Short-term temporal evolution in the light curve is also addressed. Finally, we discuss the implications for analyzing light curves of other potentially cloudy atmospheres.

2. About Neptune Light Curves

To first order, Neptune's rotational signature dominates the signature in the Kepler light curve, and stems from a few bright discrete features. Such rotational modulation has been seen in light curves with far shorter baselines in the past (e.g., Lockwood et al. 1991). Note that Neptune's internal rotation rate is actually poorly defined, and was initially based on radio emissions detected by Voyager 2 that repeated every 16.11+/- 0.05 hours (Warwick et al. 1989). Given only this brief flyby, it is still unclear if that represents the true core rotation rate; some recent studies have suggested that very stable polar cloud features may better constrain the rate to 15.96630 +/- 0.00003 hours (Karkoschka 2011). For consistency, we adopt the usual value of 16.11 hours.

Assuming the 16.11-hour rotation rate, Voyager and subsequent ground-based observations showed that Neptune's apparent zonal winds vary with latitude (*e.g.,* Sromovsky et al. 1995, 2001a, 2001b, Hammel and Lockwood 1997, Sanchez-Lavega

et al. 2015). Thus, Neptune light curves may reveal differential rotation as features at various latitudes brighten and fade. If a bright cloud feature moves with the local zonal wind, periodogram analyses can, to first order, be used to extract that cloud's latitude. A subtlety is that sometimes Neptune's brightest features actually track large disturbances at other latitudes, *e.g.*, the bright Companion Cloud to Neptune's Great Dark Spot was known to track the latitude of the dark feature, not the latitude of the bright companion itself (e.g., Smith et al. 1989, Sromovsky et al. 2011a). Thus, some caution must be exercised when extracting velocities from periodograms.

3. Kepler Light Curve Analysis

The raw Kepler data were processed by first subtracting the constant background star field. Neptune saturates the CCD, but only to the level that adjacent pixels are illuminated and photons are transferred but not lost. Thus, the signal can be summed into a disk-integrated value for each exposure. Periodic spacecraft motions and reaction wheel desaturations are removed, along with small discontinuities caused by Neptune's motion over a pixel. These corrections result in photometry with a typical noise level of about 100 parts per million or better.

The full data set includes 30-minute cadence data over a 70-day time period, but any remaining data discontinuities cannot be corrected at this cadence because real signals may be removed. However, the 49-day observations at 1-minute cadence allow for data discontinuities to be corrected. Figure 1 (top panel) shows the final extracted light curve as relative flux variations, after any remaining discontinuities and long-term trends have been removed. This curve shows a clear periodic signal, and a possible beat frequency, indicating more than one period is likely present. The curve is not perfectly smooth, with many small variations on top of the main signals. There is also some indication of time variability in the brightness and frequency of the variations (Fig. 1, bottom panel). This shows both the value, and complexity, of a long duration light curve covering ~73 rotations of the planet.

A Lomb-Scargle periodogram analysis was performed on the 49-day data set, as shown in Figure 2. Spectral power >22 indicates a false alarm probability of <0.1%. Distinct spectral power peaks are seen between 15 and 19 hours, with the most significant peaks found at 16.8, 17.9 and 18.3 hrs. None of these peaks correspond to the periods of Neptune's major moons, nor their harmonics. Horizontal oscillations detected in prior Keck observations (Martin et al. 2012), potentially linked to tidal forcing by Triton, did not produce a corresponding 7.24-hour signal in our analysis of the photometric light curve. The peaks in the periodogram, if assumed to be created by discrete cloud features, can be used to infer the latitude of those features based on a symmetric zonal wind profile (Sánchez-Lavega et al. 2015), and roughly correspond to latitudes of 45°, 28.5° and 21.5° planetographic latitude, respectively. Since the wind profile is symmetric around the equator, these results cannot distinguish between northern or southern features, and we neglect any dispersion in the zonal velocities for the moment. We can break the

hemispheric degeneracy with direct imaging observations of Neptune's cloud locations.

4. Neptune Cloud Activity During the Kepler Observations

We obtained disk-resolved imaging to provide ground-truth imaging for the photometry and to break the north-south degeneracy in the periodogram. Figure 3 shows rectilinear maps extracted from images obtained on 9 and 10 January 2015 with the Keck 2 10-meter telescope. We used the NIRC2 camera at H band (1.65 micron); this wavelength region is sensitive to relatively high clouds in the atmosphere, similar to visible red wavelength, see Figure 4. Neptune typically shows less brightness variation at wavelengths shortward of 0.7 microns, therefore red and near-infrared wavelengths show most of the atmosphere's reflected light variability from distinct clouds. Past studies have shown that discrete clouds may be at altitudes as high as the 60-230 mbar pressure level, with the main methane haze/cloud layer near 1 bar pressure and other ices (e.g., NH_3, H_2S) possible at deeper levels (higher pressures) (e.g., Sromovsky et al. 2001a).

A particularly bright discrete feature is seen at 80° W longitude in both images, although it is on the limb on the 9 Jan. image. From this single image, one cannot tell whether this is a "complex" that extends over many latitudes but moves as one feature (*e.g.*, the 1994 northern hemisphere complex; Hammel et al. 1995), or whether it is two separate features at 40° and 50° south that happen to align on this night. The very strong periodogram signature at a period corresponding to 45°, however, strongly suggests that this is indeed a "complex" that may correspond to a Great Dark Spot at 45° S, and that these bright features are companion clouds.

Another group of features that is bright and isolated enough to give a rotational signature is seen at 290° W on 9 January 2015, extending from about 30°S to 45° S. These features would also contribute to the periodogram signal at 45°. A steady smattering of features as function of longitude appears near latitude 28°S, which is consistent in the aggregate with the periodogram signature with that latitude.

The feature on 9 January at 50° west longitude (70° S) is likely the South Polar Feature (SPF) which has been imaged on numerous occasions (Smith et al. 1989, Rages et al. 2002, Karkoschka 2011). The rotation rate of this feature is quite stable at 15.97 hours (Karkoschka 2011), and does not match the zonal wind speed at this latitude, which has a period of 12.7 hours (Sanchez-Lavega et al. 2015). It is not readily observed in the Kepler periodogram, Fig. 2., though its motion is consistent with the 15.97-hour period, as is discussed later.

Comparing to the remaining features in the periodogram and their presumed latitude, there is no obvious corresponding cloud feature near 20° N or S. The Keck data were acquired near the end of the Kepler 49-day time frame, so it is possible that features may have evolved in brightness or migrated in latitude over the Kepler time frame. Additionally, the mean wind profile may not be an accurate

representation of the velocity of the visible features, as is noted for the SPF. Lastly, these images do not represent the visible wavelength appearance of the planet (which senses a lower altitude) from which we derive the light curve.

5. Other Neptune Observations

Hubble data were also acquired in September 2015 as part of the *"Hubble 2020: Outer Planet Atmospheres Legacy"* (OPAL) program (Simon et al. 2015). The OPAL program generates two global Neptune maps each year using the Wide Field Camera 3 (WFC3). A main goal of OPAL is to provide Neptune data for long duration time-domain studies of cloud activity and wind field variability, making it a perfect companion to this work. Although the data were acquired well after the Kepler observations, they enable an independent high-spatial-resolution look at the clouds at visible and near-IR wavelengths to show how much they vary over 9 months.

Figure 5 shows Hubble observations of a complete rotation of Neptune, created from 4 orbits. Very similar cloud structure is seen in the Keck H-band (Fig. 3) and Hubble 845-nm (Fig. 5, top), epochs, including the large storms system near latitude 45° S and the bright SPF at latitude 70° S. However, fewer features are also observed near 25° N, implying some variability since January 2015. The color comparison (bottom panel in Fig. 5) shows that many of the cloud features are muted at shorter visible wavelengths, and darker bands also appear between 40° to 50° S and 60° to 70° S. Thus, a panchromatic visible light curve would be dominated by the variable clouds at the longer wavelengths (*i.e.*, by the features that appear white in the composite).

Observations of a second rotation of the planet were not completed due to a spacecraft tracking anomaly; only part of the second map was obtained leaving a longitude gap from 235 to 308° W. However, many of the cloud features were captured, allowing for feature motion measurements; these generally match the wind profile in Fig. 5, with the exception of the SPF. Small variations are expected, as larger cloud features can also have internal rotation and drift rates that do not represent the mean zonal wind. This is particularly true of the SPF, which drifts at a much slower rate than the zonal wind at that latitude. Previous cloud motion measurements indicate velocity dispersions of 200 m/s or higher, indicating much variability in feature motions; it is unclear if this also applies to the true zonal wind field as feature motions may not be identical to the zonally averaged wind (Martin et al. 2012, Fitzpatrick et al. 2014).

In addition, the 845-nm filter was sampled repeatedly within the orbits, giving additional coverage of features and full disk measurements. Some small changes in cloud morphology were observed, but these are unlikely to affect a disk-integrated light curve. However, 25 exposures were obtained in the 845-nm filter, as it was repeated throughout each orbit, and we used the full-disk brightness to generate the light curve shown in Figure 6 (see the Supplemental Online Material for a full animation of the images and light curve). Although a periodic signal with a

minimum to maximum amplitude of ~16% can be seen in this light curve, a Lomb-Scargle periodogram cannot pull out a unique period because of the sparse coverage. The dashed line indicates the 16.8-hour period expected if the 45° S feature dominated this light curve, and red and blue curves show normalized Kepler light curves from Days 6 and 25, respectively. The Hubble light curve represents the maximum variation we would expect to see, as cloud contrast is maximized. Full disk counts in the 467-nm filter, from the darkest to brightest views, give a 0.2% variation in total integrated counts, at the limit of the WFC3 photometric accuracy (Kalirai et al. 2009, 2010).

The smaller cloud signal observed at shorter wavelengths is due to the atmospheric levels sensed by these filter bandpasses, as shown in Fig. 4. The shortest wavelengths are dominated by Rayleigh scattering, which gives an overall bright atmospheric background, reducing contrast for discrete cloud features. At longer wavelengths, Rayleigh scattering is reduced and particle scattering above the 1-bar pressure level can be more easily detected. At methane and other gas absorption bands, photons are absorbed before reaching deeper cloud levels, and higher clouds show high contrast from the rest of the atmosphere, for example at 890 nm. Thus, at shorter wavelengths, or with a panchromatic visible bandpass, the light signal from discrete clouds is much more muted than at red and infrared continuum or absorption band wavelengths.

6. Discussion

The data acquired in 2015 from Keck and Hubble show that the planet varies on a timescale of hours to months. The largest feature, at 45° S has been quite stable, however, as have the location of some of the bands of cloud activity. On the other hand, the planet can show dramatic variability in clouds. Figure 7 shows a similar map from Hubble data acquired in 2011 at 845 nm. Here there are no complete bands of clouds, but many more discrete clouds. During the Voyager 2 flyby in 1989 there were few bright clouds, and Neptune's dominant cloud features were the Great Dark Spot near ~15° S, the SPF near 70° S, another dark spot near 55° S and a bright cloud near 45° S (Smith et al. 1989). However, Neptune's more usual appearance includes bands of activity with discrete storms. Table 1 provides an incomplete summary of cloud activity on Neptune over the past 20 years to show that some latitudes have fairly constant cloud activity, but many more evolve with time. In several of these cases, cloud evolution was seen over just a few days or even hours (Sromovsky 2001b, Fitzpatrick 2014).

Table 1. A limited 20-year summary of cloud detections

Date	Facility	North	South	Reference
1994	Hubble	Discrete dark feature at 30°, bright features at	Bright features at 30° and 45° S	Hammel et al. 1995

		27° N to equator		
1996	Hubble/ NASA's IRTF	Discrete features near 20° to 40° N	Bands near 20° to 40° w/ features, feature near 60° S	Sromovsky et al. 2001a
1998	Hubble	Features between 20° and 50° N	Band near 45°, features at 15° to 40° S	Sromovsky et al. 2001b
2001	Keck	Band at 28° N, sporadic bright clouds at 36° N	Bands at 23°, 31°, 36°, 45° and 49° S	Martin et al. 2012
2001	Hubble		Bright feature at 70° S	Rages et al. 2002
2003	Keck, VLA	Bands between 25° and 40° N	Bands between 30° and 50° S, discrete features near 60-70° S	de Pater et al. 2014
2009	Keck	Bands at mid latitudes, features at 40° N	Large feature at 65° S	Fitzpatrick et al. 2014
2011	Hubble	Broken bands, many features	Broken bands, features from 10 to 50° S	*this paper*
Jan. 2015	Keck	Bands from 25° to 40° N	30° S, features at 40° to 50° S	*this paper*
Sep. 2015	Hubble	Broken band 30° to 40° N, features at 20° N	Bands from 25° to 40° S, features at 45° and 70° S	*this paper*

In addition to changing cloud activity, it has been noted that longer-lived features can oscillate in latitude and longitude. Larger features in the Voyager 2 images showed that features near 21°, 42° and 54° S latitude could oscillate by 2° to 4° latitude and 8° of longitude (Sromovsky 1991). With the long Kepler coverage, it is possible that different periods, corresponding to different latitudes, could be found if binned over smaller time intervals rather than searched over the entire 49-day duration. Figure 8 shows the same Lomb-Scargle periodogram analyses run over 3.5-day intervals (5.25 Neptune rotations).

Significant spectral power is seen in every segment, but none show multiple peaks, and the variations are too large to represent a single cloud feature's motion. Rather, different features may dominate on different days, as they brighten or spread and then dissipate. For example, the signature of the 70° S feature may be dominating the signal at Days 45-49, even though it is not seen in the full periodogram in Fig. 2. This is not unusual, as observations from Keck and Hubble over 2000 to 2001 showed that the SF features can come and go, evolving on timescales as short as 30

hours and visible in about 20% of observations (Rages et al. 2002). Additionally, noise may be preventing clean retrievals of multiple features over so few rotations of the planet.

The observed Neptune variability has implications for brown dwarf light curve analyses. While some brown dwarfs show remarkably consistent light curves (e.g., Gizis et al. 2015 and examples cited therein), the light curves of other brown dwarfs evolve with time. In their study with the Spitzer Space Telescope of photometric variability of L3-T8 dwarfs, Metchev et al. (2015) found that about half were variable in IRAC bands 1 and 2 and of these about 1/3 showed rapid light curve evolution (over timescales of hours).

The largest amplitude variability among brown dwarfs occurs at the L to T type transition where the thick cloudy atmospheres of the late L dwarfs transition to the relatively cloud free spectra of the mid to late T dwarfs. For example, the J band thermal emission of the T2.5 brown dwarf SIMP J013656.57+093347.3 shows peak to valley variations as large as 5% with a period of a few hours (Artigau et al. 2009). The dwarf's light curve clearly evolves with time, exhibiting clear morphological differences in a few dozen rotations. Artigau et al. (2009) attribute the variations to evolution of patches of clear and cloudy regions in the atmosphere. Likewise Radigan et al. (2012) found large (26%) variations in the JHK thermal flux from the T1.5 dwarf 2MASS J21392676+ 0220226 with a period of about 8 hours. The light curve shape of this object also evolves over a few rotation period and Radigan et al. also attribute this to evolving photospheric clouds.

In perhaps the best known example of T dwarf variability, Gillon et al. (2013) monitored the L7.5/T0.5 binary WISE J104915.57-531906.1, commonly known as Luhman 16AB. They found 11% variability in the atmosphere of the cooler (T0.5) component that notably evolved over 12 nights of observations. Crossfield et al. (2014) later used Doppler imaging techniques to resolve individual bright and dark spots over the disk of the T dwarf, supporting the interpretation that photospheric clouds were responsible both for the periodic modulation of the light curve as well as its evolution in time.

It is interesting to consider the light curve evolution of Neptune in this context. First, it is worth repeating that the Neptune variability detected by K2 arises not from variations in the thermal flux but rather the distribution and reflectivity of the global cloud deck (although temperature contrasts within the atmosphere may well play a role in the evolution of the cloud features). The main component of the Neptune light curve (Fig. 1) is the dramatic bright spot and this feature is long lived and is responsible for the principal component of the variation over a single rotation (Fig. 2). However, multiple smaller features both produce irregularities in the light curve and seem to evolve over more rapid timescales, at time as quickly as within a rotation or two (Fig. 8). Without the large spot the light curve would be far more irregular, and without the varying smaller spots the rapidity of the evolution would be much less.

Stellar spot modeling (e.g., Mosser et al. 2009, Karalidi et al. 2015) can extract latitude information depending on the stellar inclination, and assumptions about spot size and albedo. At 90° inclination, no transits/modulations are seen, and at zero inclination, all spots transit in half a rotation period; other inclinations allow reasonably constrained retrieval of spot latitude to +/- 10° to +/- 20° (Mosser et al. 2009). As Neptune has a tilt of 28°, this type of spot-latitude modeling would provide an interesting comparison to our work.

It should also be noted, however, that Neptune has large, latitude-dependent zonal wind velocities of several hundred meters per second, and some clouds move at the corresponding zonal velocity, while others do not. Without prior knowledge of Neptune's zonal wind field, we could not exact assign latitudes to any particular period in the light curve, and no features appeared at the presumed 16.11-hour rotation period. For comparison, Jupiter has lower maximum zonal velocities (~150 m/s), lower obliquity (3°), and its storms typically drift at lower velocity than the corresponding zonal winds (e.g., Beebe et al. 1989, Simon and Beebe 1996). Here, modeling a short duration light curve does extract Jupiter's rotation rate and Great Red Spot latitude, though other spots are not obvious due to small size, low contrast, and degeneracy in the latitude retrievals (Karalidi et al 2015). In principle, longer cadences could provide some zonal wind information, at least for latitudes with high contrast, distinct, cloud features, though they will be biased by the storm's own motions. This highlights the importance of simultaneous, resolved, imaging when possible.

Perhaps the diversity seen among brown dwarf light curves, with some exhibiting relatively stable sinusoidal variations while others show either no regularity or rapidly evolve, is likewise a consequence of the balance of large, high contrast, and smaller, more dynamic features. A logical next step would be to compare the observed Neptune variations to the predictions of a global climate model that could investigate the atmospheric dynamics both of irradiated giant planets and brown dwarfs, as well as to study long duration light curves from the other solar system giant planets. A statistical study of the types of weather patterns and their resulting variability would inform discussions such as these.

Acknowledgements

This paper includes data collected by the Kepler mission. Funding for the Kepler mission is provided by the NASA Science Mission Directorate. This work was based, in part, on observations made with the NASA/ESA Hubble Space Telescope under programs GO12675 and GO13937. Support for program GO13937 was provided by NASA through a grant from the Space Telescope Science Institute, which is operated by the Association of Universities for Research in Astronomy, Inc., under NASA contract NAS5-26555. Some of the data presented herein were obtained at the W.M. Keck Observatory, which is operated as a scientific partnership among the California Institute of Technology, the University of California and the National Aeronautics and Space Administration. The Observatory was made possible by the generous financial support of the W.M. Keck Foundation. We thank

Danielle Piskorz, Henry Ngo, and Heather Knutson for acquiring the Keck images of Neptune. The authors wish to recognize and acknowledge the very significant cultural role and reverence that the summit of Mauna Kea has always had within the indigenous Hawaiian community. We are most fortunate to have the opportunity to conduct observations from this mountain.

References:

Apai, D., J. Radigan, E. Buenzil, A. Burrows, I. N. Reid, R. Jayawardhana (2013) HST Spectral Mapping of L/T Transition Brown Dwarfs Reveals Cloud Thickness Variations. *Astrophys J.* **768**, 121. DOI: 10.1088/0004-637X/768/2/121

Artigau, E., S.Bouchard, R. Doyon, D. Lafreniere (2009) Photometric Variability of the T2.5 Brown Dwarf SIMP J013656.5+093347: Evidence for Evolving Weather Patterns. *Astrophys. J.*, **701**, 1534. DOI: 10.1088/0004-637X/701/2/1534

Bailer-Jones, C.A.L and R. Mundt (2001). Variability in ultra cool dwarfs: Evidence for the evolution of surface features. *Astronomy and Astrophysics* **367**, 218. DOI: 10.1051/0004-6361:20000416.

Batalha, N. M. (2014). Exploring exoplanet populations with NASA's Kepler Mission. *PNAS* **111**, 12647-12654. DOI: 10.1073/pnas.1304196111

Beebe, R. F., G. S. Orton, R. A. West (1989). Time-Variable Nature of the Jovian Cloud Properties and Thermal Structure: an Observational Perspective in *Time Variable Phenomenon in the Jovian System*. NASA-SP-494, 285.

Burrows, A., W.B. Hubbard, J.I.Lunine, J. Liebert (2001) The theory of brown dwarfs and extrasolar giant planets. *Rev. Modern Physics*. **73**, 719. DOI: 10.1103/RevModPhys.73.719

Cassini, G. (1665). Some Observations Concerning Jupiter. Of the Shadow of One of His Satellites, Seen by a Telescope Passing Over the Body of Jupiter. *Philosophical Transactions* **1**, 143.

Chabrier, G., I. Baraffe, F. Allard, and P. Hauschildt (2000). Evolutionary Models for Very Low-Mass Stars and Brown Dwarfs with Dusty Atmospheres. *ApJ* **542** 464. DOI: 10.1086/309513

Crossfield, I.J.M., B. Biller, J.E. Schlieder, N. R. Deacon, M. Bonnefoy, D. Homeier, F. Allard, E. Buenzli, T. Henning, W. Brandner,B. Goldman, T. Kopytova (2014). A global cloud map of the nearest known brown dwarf. *Nature* **505**, 654. DOI: 10.1038/nature12955

de Pater, I., L. N. Fletcher, S. Luszcz-Cook, D. DeBoer, B. Butler, H. B. Hammel, M. L. Sitko, G. Orton, P. S. Marcus (2014). Neptune's global circulation deduced from multi-wavelength observations. *Icarus* **237**, 211–238. DOI: 10.1016/j.icarus.2014.02.030

Dressel, L. (2015). Wide Field Camera 3 Instrument Handbook, Version 7.0. (Baltimore: STScI)

Fitzpatrick, P.J., I. de Pater, S.H. Luszcz-Cook, M.H. Wong, H.B. Hammel (2014). Dispersion in Neptune's zonal wind velocities from NIR Keck AO observations in July 2009. *Astrophys Space Sci*. **350**, 65–88. DOI: 10.1007/s10509-013-1737-2

Gelino, C.R. and M.S. Marley (2000). Variability in an Unresolved Jupiter in *From Giant Planets to Cool Stars* (C. Griffith, M. Marley, eds.), ASP Conference Series 212, 322

Gelino, C.R., M.S. Marley, J.A. Holtzman, A.S. Ackerman, K. Lodders (2002). L Dwarf Variability: I-Band Observations. *Astrophys. J*. **577**, 433. DOI: 10.1086/342150

Gillon, M., A.H.M. Triaud, E. Jehin, L. Delrez, C. Opitom, P. Magain, M. Lendl, D Queloz (2013.) Fast-evolving weather for the coolest of our two new substellar neighbours. *Astron. & Astrophys*. **555**, L5. DOI: 10.1051/0004-6361/201321620

Gizis, J.E, K.G. Dettman, A. J. Burgasser, S. Camnasio, M. Alam, J.C. Filippazzo, K.L. Cruz, S. Metchev, E. Berger, and P.K.G. Williams (2015). Kepler Monitoring of an L Dwarf II. Clouds with Multiyear Lifetimes. *Astrophys. J*., accepted.

Hammel, H.B. and G.W. Lockwood (1997). Atmospheric structure in 1994, 1995, and 1996: HST imaging at multiple wavelengths. *Icarus* **129**, 466–481.

Hammel, H. B., G. W. Lockwood, J. R. Mills, and C. D. Barnet (1995). Hubble Space Telescope imaging of Neptune's cloud structure in 1994. *Science* **268**, 1740-1742.

Howell, S.B. et al. (2010). The K2 Mission: Characterization and Early Results. *PASP* **126**, 398. DOI: 10.1086/676406.

Joyce, R.R., C.B. Pilcher, D.P. Cruikshank, D. Morrison (1977). Evidence for weather on Neptune: I. *Astrophys. J*. **214,** 657. DOI: 10.1086/155291.

Kalirai, J.S., J. MacKenty, A. Rajan S. Baggett, R. Bohlin, T. Brown, S. Deustua, R. A. Kimble, A. Riess, E. Sabbi, and the WFC3 Team (2009). WFC3 SMOV Proposal 11450: The Photometric Performance and Calibration of WFC3/UVIS. STScI Instrument Science Report WFC3 2009-31.

Kalirai, J. S., S. Baggett, T. Borders, and A. Rajan (2010). The Photometric Performance of WFC3/UVIS: Temporal Stability Through Year 1. STScI Instrument Science Report WFC3 2010-14.

Karalidi, T., D. Apai, G. Schneider, J.R. Hanson, J. M. Pasachoff (2015). Aeolus: A Markov-Chain Monte Carlo code for mapping ultracool atmospheres. An application on Jupiter and brown dwarf HST light curves. *ApJ*, accepted.

Karkoschka, E. (2011). Neptune's rotational period suggested by the extraordinary stability of two features. Icarus 215, 439. DOI: 10.1016/j.icarus.2011.05.013

Koch, D.G. et al. (2010). Kepler Mission Design, Realized Photometric Performance, and Early Science. *Astrophysical Journal Letters* **713**, L79. DOI: 10.1088/2041-8205/713/2/L79

Marley, M.S., A.S. Ackerman, J.N. Cuzzi, D. Kitzmann (2013). Clouds and Hazes in Exoplanet Atmospheres (The University of Arizona Press), 367.

Martin, S. C., I. de Pater, P. S. Marcus (2012). Neptune's zonal winds from near-IR Keck adaptive optics imaging in August 2001. *Astrophys Space Sci* **337**, 65–78. DOI: 10.1007/s10509-011-0847-y

Metchev, S.A., A. Heinze, D. Apai, D. Flateau, J. Radigan, A. Burgasser, M.S. Marley, E. Artigau, P. Plavchan, B. Goldman (2015). Weather on Other Worlds. II. Survey Results: Spots are Ubiquitous on L and T Dwarfs. *Astrophys. J*. **799**, 154. DOI: 10.1088/0004-637X/799/2/154

Mosser, B., F. Baudin, A. F. Lanza, J. C. Hulot, C. Catala, A. Baglin, and M. Auvergne (2009). Short-lived spots in solar-like stars as observed by CoRoT. *Astronomy and Astrophys*. **506**, 245. DOI: 10.1051/0004-6361/200911942

Radigan, J., R. Jayawardhana, D. Lafreniere, E. Artigau, M.S. Marley, D. Saumon (2012). Large-amplitude Variations of an L/T Transition Brown Dwarf: Multi-wavelength Observations of Patchy, High-contrast Cloud Features. *Astrophys. J*. **750**, 105. DOI: 10.1088/0004-637X/750/2/105

Radigan, J. D. Lafreniere, R. Jayawardhana, E. Artigau (2014). Strong Brightness Variations Signal Cloudy-to-Clear Transition of Brown Dwarfs. *Astrophys. J*. **793**, 75. DOI: 10.1088/0004-637X/793/2/75.

Rages, K., H.B. Hammel, G.W. Lockwood (2002). A prominent apparition of Neptune's South Polar Feature. *Icarus* **159**, 262–265. DOI: 10.1006/icar.2002.6900

Rowe, J. F., J.M. Matthews, S. Seager, D. Sasselov, R. Kuschnig, D. B. Guenther, A.F.J. Moffat, S.M. Rucinski, G.A.H. Walker, W. W. Weiss (2009). Towards the Albedo of an Exoplanet: MOST Satellite Observations of Bright Transiting Exoplanetary Systems. *Proceedings of the International Astronomical Union, IAU Symposium 253*, **4**, 121-127. DOI: http://dx.doi.org/10.1017/S1743921308026318

Simon, A. A and R. F. Beebe (1996). Jovian Tropospheric Features - Wind Field, Morphology and Motion of Long-lived Systems. *Icarus* **121**, 319-330

Simon, A.A., M.H. Wong, and G.S. Orton (2015). First results from the Hubble OPAL Program: Jupiter in 2015. *Astrophysical Journal* **812**, 55. DOI: 10.1088/0004-637X/812/1/55

Smith, B. A., L. A. Soderblom, D. Banfield, C. Barnet, A. T. Basilevksy, R. F. Beebe, K. Bollinger, J. M. Boyce, A. Brahic, G. A. Briggs, R. H. Brown, C. Chyba, S. A. Collins, T. Colvin, A. F. Cook II, D. Crisp, S. K. Croft, D. Cruikshank, J. N. Cuzzi, G. E. Danielson, M. E. Davies, E. De Jong, L. Dones, D. Godfrey, J. Goguen, I. Grenier, V. R. Haemmerle, H. Hammel, C. J. Hansen, C. P. Helfenstein, C. Howell, G. E. Hunt, A. P. Ingersoll, T. V. Johnson, J. Kargel, R. Kirk, D. I. Kuehn, S. Limaye, H. Masursky, A. McEwen, D. Moriuson, T. Owen, W. Owen, J. B. Pollack, C. C. Porco, K. Rages, P. Rogers, D. Rudy, C. Sagan, J. Schwartz, E. M. Shoemaker, M. Showalter, B. Sicardy, D. Simonelli, J. Spencer, L. A. Sromovsky, C. Stoker, R. G. Strom, V. E. Suomi, S. P. Synotr, R. J. Terrile, P. Thomas, W. R. Thompson, A. Verbiscer, J. Veverka (1989). Voyager 2 at Neptune: Imaging Science Results. *Science* **246**, 1422, DOI: 10.1126/science.246.4936.1422

Sromovsky, L. A. (1991). Latitudinal and Longitudinal Oscillations of Cloud Features on Neptune. *Science* **254**, 684-686. DOI: 10.1126/science.254.5032.684

Sromovsky, L. A., P. M. Fry, T. E. Dowling, K. H. Baines, S. S. Limaye (2001a). Coordinated 1996 HST and IRTF Imaging of Neptune and Triton III. Neptune's Atmospheric Circulation and Cloud Structure. *Icarus* **149**, 459–488. doi:10.1006/icar.2000.6564

Sromovsky, L. A., P. M. Fry, T. E. Dowling, K. H. Baines, S. S. Limaye (2001b). Neptune's Atmospheric Circulation and Cloud Morphology: Changes Revealed by 1998 HST Imaging. *Icarus* **150**, 244–260. doi:10.1006/icar.2000.6574.

Sromovsky, L.A., S.S. Limaye, P.M. Fry (1995). Clouds and circulation on Neptune: Implications of 1991 HST observations. *Icarus* **118**, 25–38. DOI: 10.1006/icar.1995.1175

Sromovsky, L.A., P.M. Fry, K.H. Baines, T.E. Dowling, T.E. (2001c). Coordinated 1996 HST and IRTF imaging of Neptune and Triton. II. Implications of disk-integrated photometry. *Icarus* **149**, 435–458. DOI: 10.1006/icar.2001.6563.

Sánchez-Lavega, A., L. Sromovsky, A. Showman, A. Del Genio, R. Young, R. Hueso, E. García Melendo, Y. Kaspi, G.S. Orton, N. Barrado-Izagirre, D. Choi, J. Barbara (2015). Zonal Jets in Gas Giants, in *Zonal Jets*. B. Galperin and P.L. Read, eds., Cambridge University Press, Cambridge, in press.

Tinney, C.G. and A.J. Tolley (1999). Searching for weather in brown dwarfs. *MNRAS* **304**, 119. DOI: 10.1046/j.1365-8711.1999.02297.x

Warwick, J., D. R. Evans, G. R. Peltzer, R. G. Peltzer, J. H. Romig, C. B. Sawyer, Anthony C. Riddle, A. E. Schweitzer, M. D. Desch, M. L. Kaiser, W. M. Farrell, T. D. Carr, I. De Pater, D. H. Staelin, S. Gulkis, R. L. Poynter, A. Boischot, F. Genova, Y. Leblanc, A. Lecacheux, B. M. Pedersen, P. Zarka (1989). Voyager Planetary Radio Astronomy at Neptune. *Science* **246**, 1498-1501. DOI: 10.1126/science.246.4936.1498

Yang, H., D. Apai, M.S. Marley, D. Saumon, C.V. Morley, E. Buenzli, E. Artigau, J. Radigan, S. Metchev, A. J. Burgasser, S. Mohanty, P.J. Lowrance, A.P. Showman[2], T. Karalidi, D. Flateau, and A.N. Heinze (2015). *HST* Rotational Spectral Mapping Of Two L-Type Brown Dwarfs: Variability In And Out Of Water Bands Indicates High-Altitude Haze Layers. *Astrophys. J. Lett.* **798**, L13. DOI: 10.1088/2041-8205/798/1/L13

Figure Captions:

Figure 1. The Kepler light curve of Neptune. The top panel shows the full 49-day light curve, with normalized brightness variations. The bottom panel shows several 5-day segments emphasizing the evolution of brightness variations with time.

Figure 2. Lomb-Scargle periodogram of Neptune derived from 49 days of Kepler observations. The retrieved periodic signals are labeled with latitudes corresponding to that rotation period based on the zonal velocity curve given by Sanchez-Lavega et al. (2015); the features could be in either hemisphere. Our assumed Neptune internal rotation rate (velocity = 0 m/s) is shown by the dashed line (16.11 hrs, Warwick et al., 1989).

Figure 3. Keck H-band images of Neptune from 9-10 January 2015, covering most longitudes. The top panels are unmapped images, and the bottom panels show the latitude and longitude coverage mapped at 2 pixels per degree. These show typical Neptune structure: bright bands of Neptunian cloud activity from planetographic latitude 25° to 40° in the northern and southern mid-latitudes, with occasional brighter features.

Figure 4. Spectral sensitivity and atmospheric transmission. Labeled curves show the total spectral sensitivity of Kepler and HST observations (Koch et al. 2010, Dressel 2015). The Keck infrared bandpass includes NIRC2 H-band filter transmission and detector quantum efficiency, but neglects the telescope optical path outside NIRC2. The atmospheric penetration depth, right axis, is the pressure level where a two-way optical depth of unity is reached in a cloud-free model of Neptune's atmosphere, including opacity from Rayleigh scattering and gas absorption (from Sromovsky et al. 2001a).

Figure 5. Hubble map of Neptune acquired 18 September 2015. The top panel shows a global map constructed from 845-nm images. The bottom is a visible-wavelength color-composite map (with the blue, green, and red channels mapped to 467, 547, and 657 nm, respectively). We overplot the smoothed zonal wind profile (Sánchez-Lavega et al. 2015), showing winds up to 400 m/s (top axis).

Figure 6. Light curve of Neptune from Hubble full-disk brightness at 845 nm (plus signs). A sinusoidal variation, with a 16.8-hour period and arbitrary amplitude, is shown by the dashed line. For comparison, normalized Kepler light curves beginning at Day 6 and Day 25 are shown in blue and red, respectively.

Figure 7: Neptune global map from Hubble WFC3/UVIS acquired 25-26 June 2011 at 845 nm. High northern latitudes were not visible, and a bad column resulted in artifacts at high southern latitudes; no SPF is visible.

Figure 8. Short-interval periodogram analysis. The top panel shows the Lomb-Scargle periodogram in 3.5-day segments; red indicates higher spectral power. The remaining panels show the Kepler brightness variations (black curves) from three of the segments, phased to the corresponding period of maximum spectral power from the periodogram, and plotted over two rotations within that interval; the most significant period is shown as a dashed red line for each date.

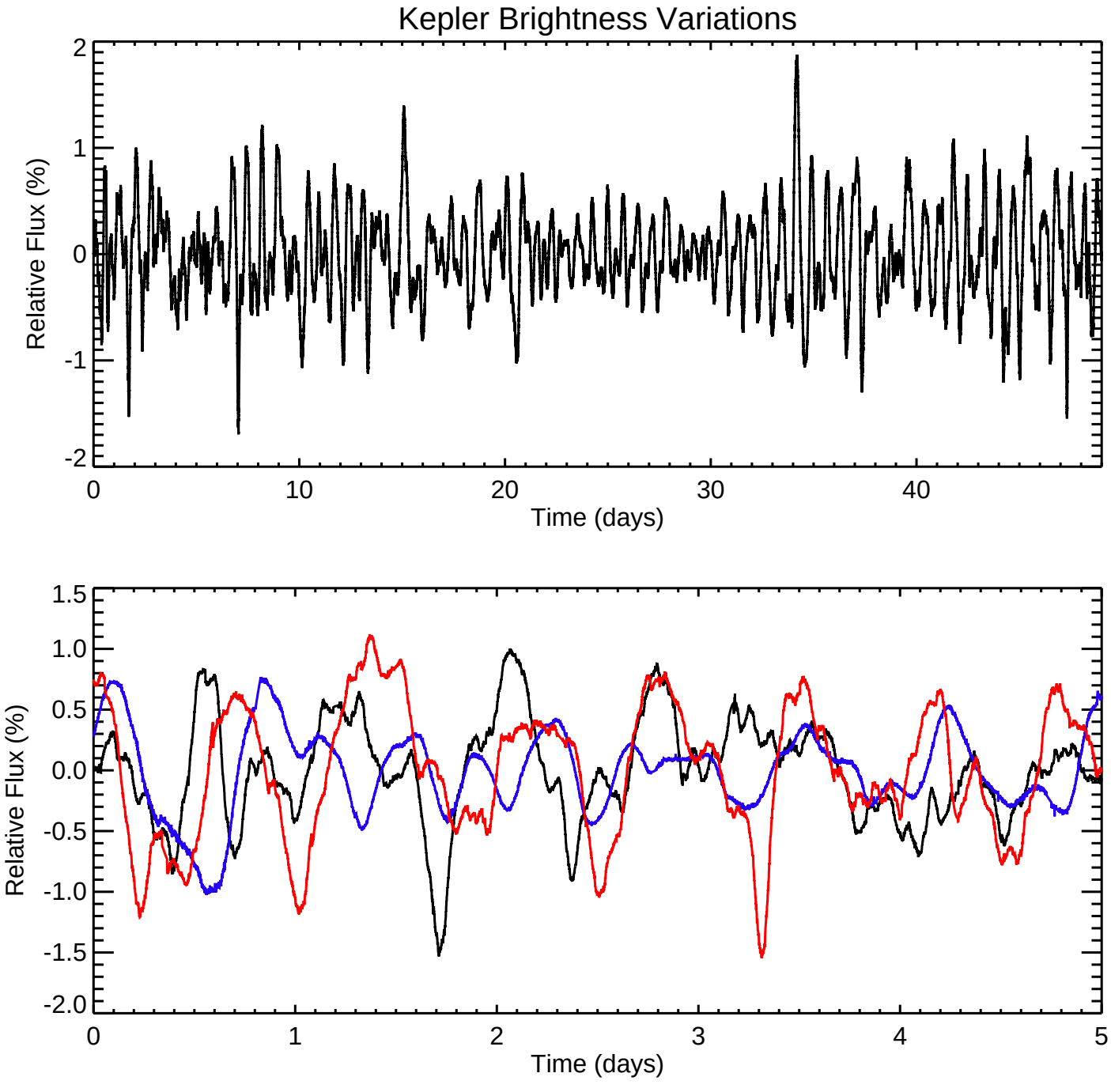
Kepler Brightness Variations
Relative Flux (%)
2
1
0
-1
-2
0
10
20
30
40
Time (days)
Relative Flux (%)
1.5
1.0
0.5
0.0
-0.5
-1.0
-1.5
-2.0
0
1
2
3
4
5
Time (days)

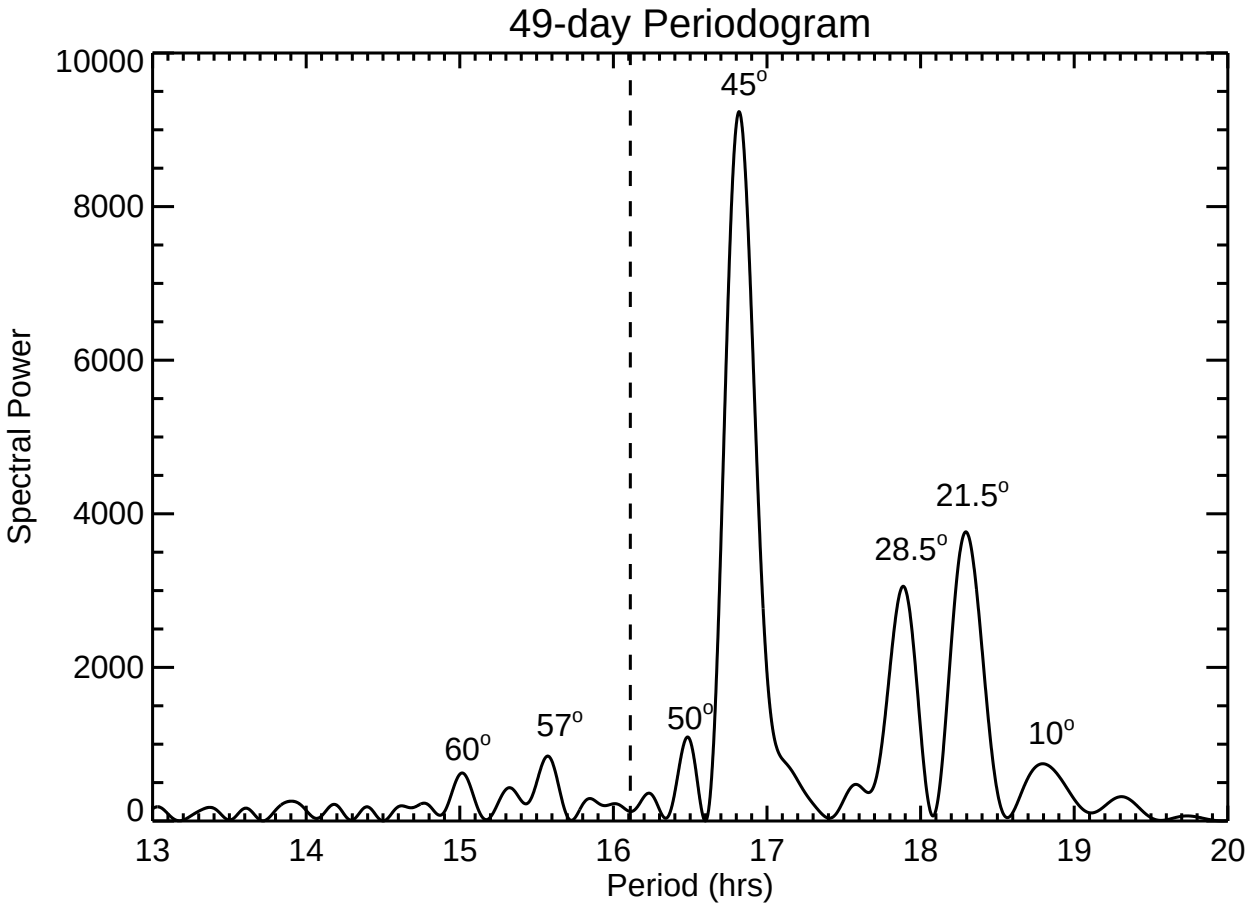
49-day Periodogram
Spectral Power
Period (hrs)
10000
8000
6000
4000
2000
0
13
14
15
16
17
18
19
20
45°
60°
57°
50°
28.5°
21.5°
10°

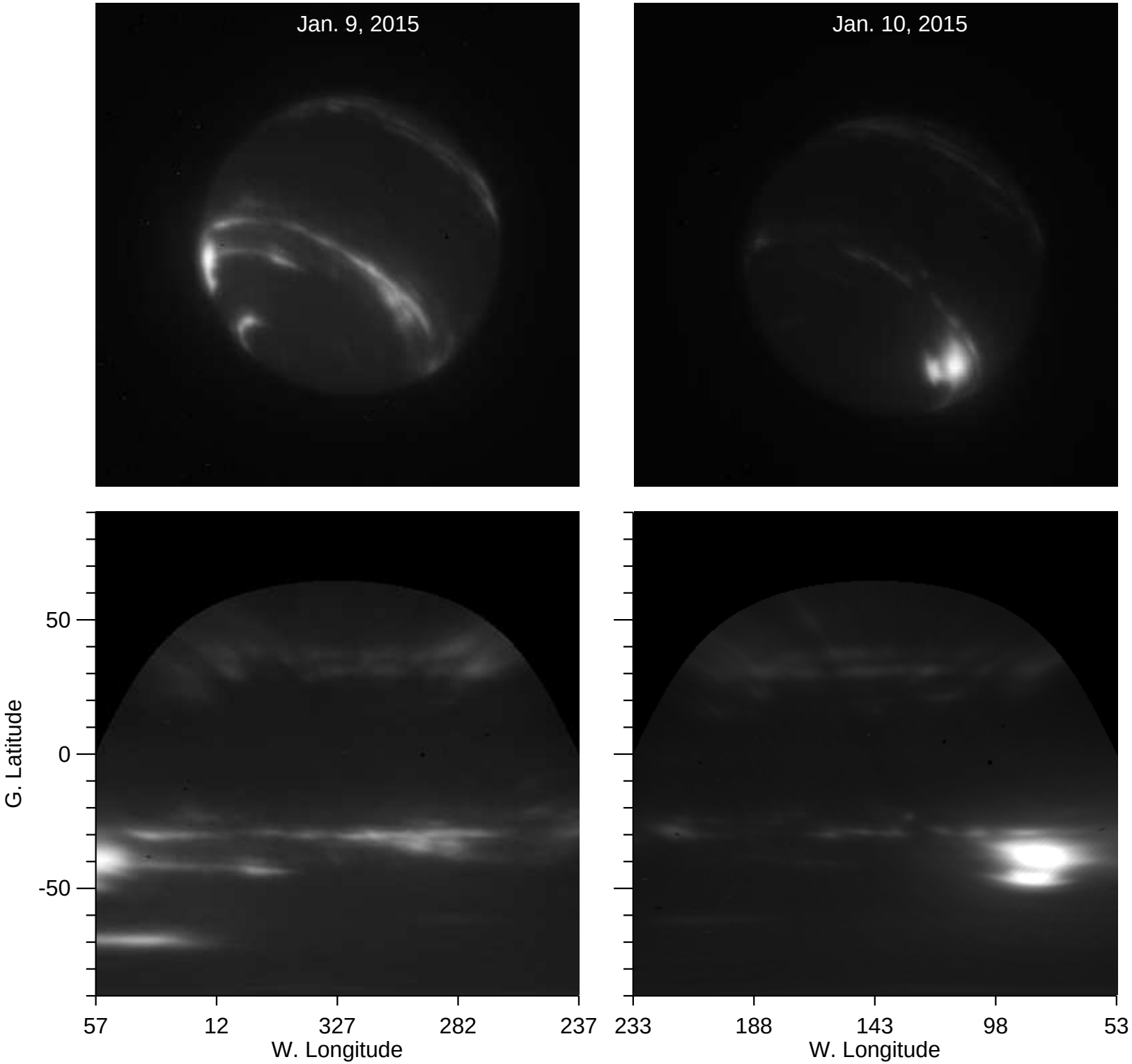
Jan. 9, 2015
Jan. 10, 2015
50
0
-50
G. Latitude
57
12
327
282
237
W. Longitude
233
188
143
98
53
W. Longitude

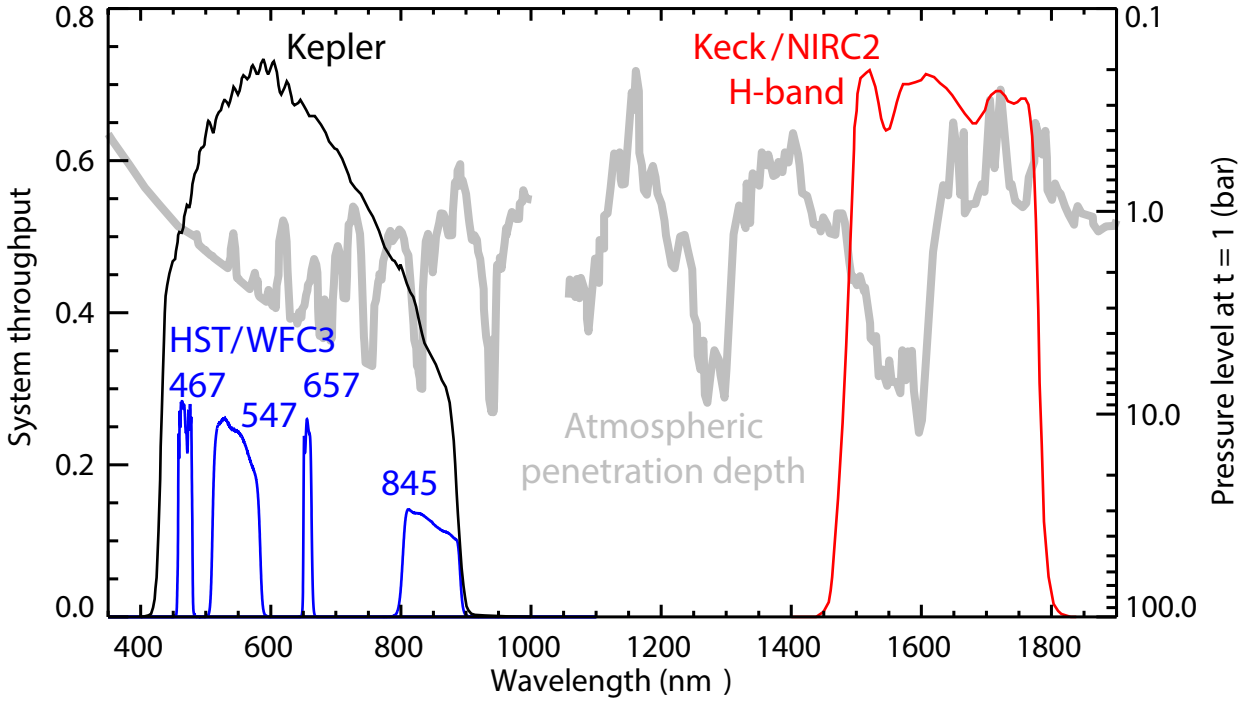
Kepler
Keck / NIRC2
H-band
HST/WFC3
467
547
657
845
Atmospheric
penetration depth
System throughput
Pressure level at t = 1 (bar)
Wavelength (nm)
0.0
0.2
0.4
0.6
0.8
0.1
1.0
10.0
100.0
400
600
800
1000
1200
1400
1600
1800

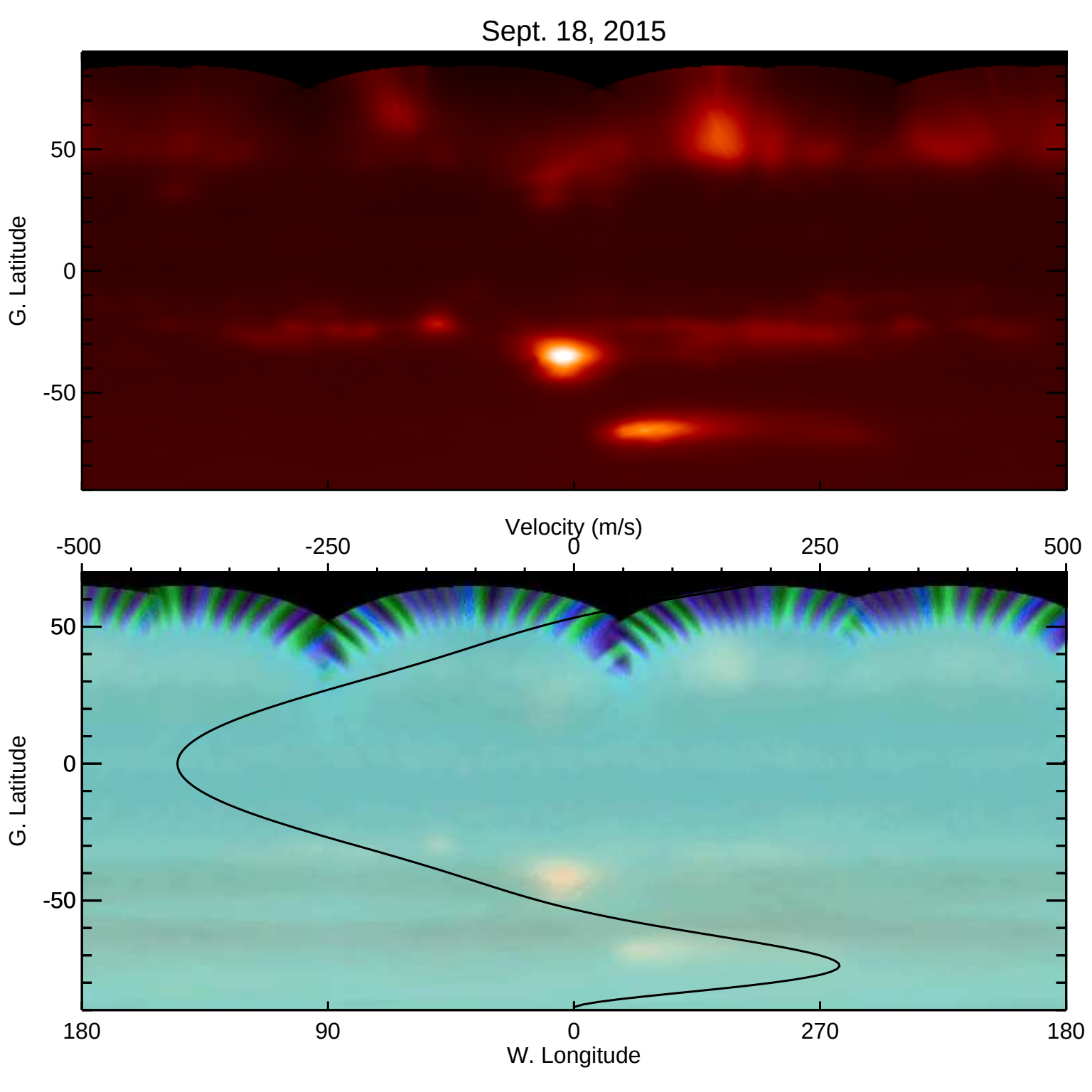
Sept. 18, 2015
G. Latitude
50
0
-50
Velocity (m/s)
-500
-250
0
250
500
G. Latitude
50
0
-50
180
90
0
270
180
W. Longitude

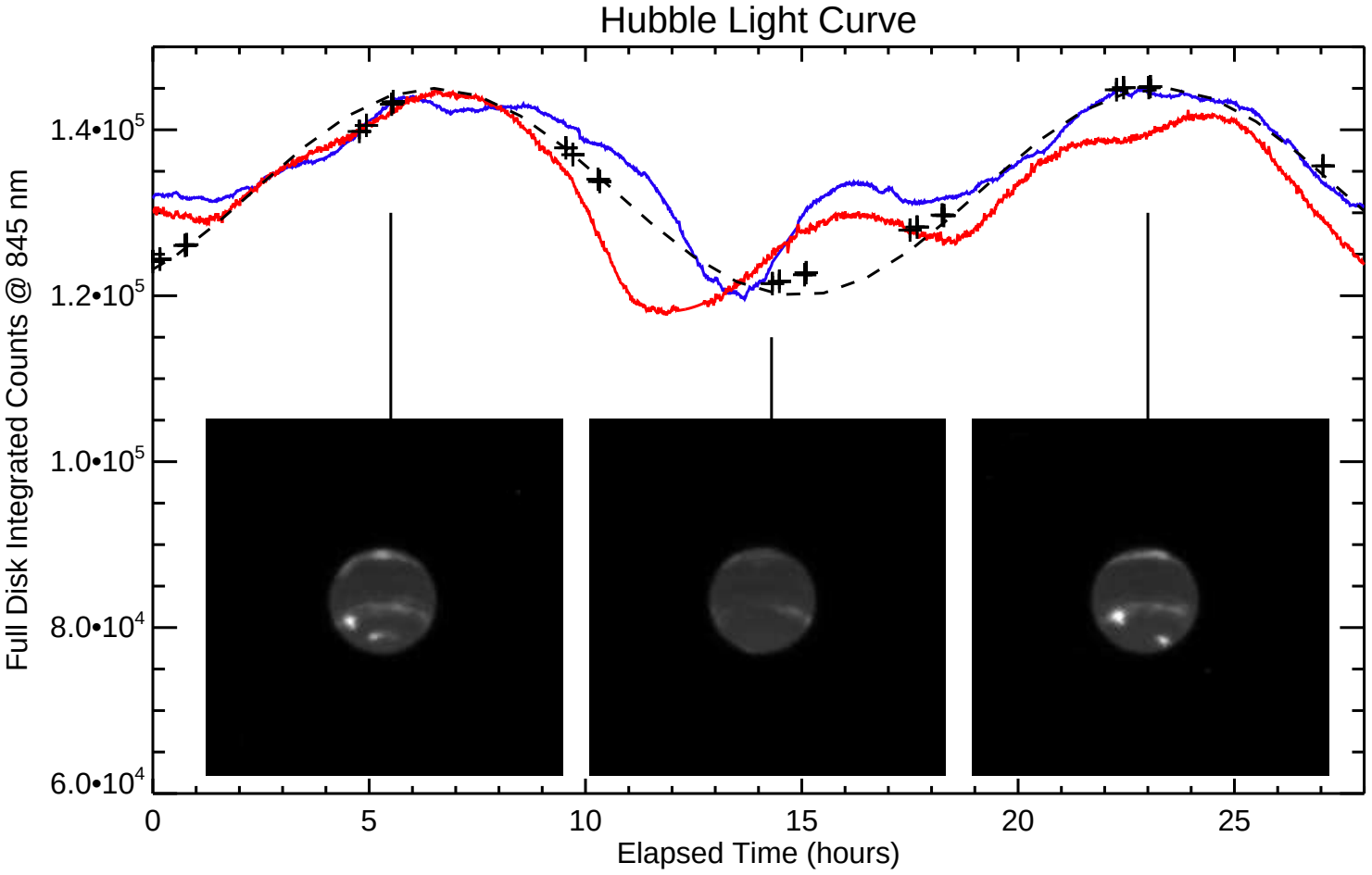
Hubble Light Curve
Full Disk Integrated Counts @ 845 nm
1.4•10^5
1.2•10^5
1.0•10^5
8.0•10^4
6.0•10^4
0
5
10
15
20
25
Elapsed Time (hours)

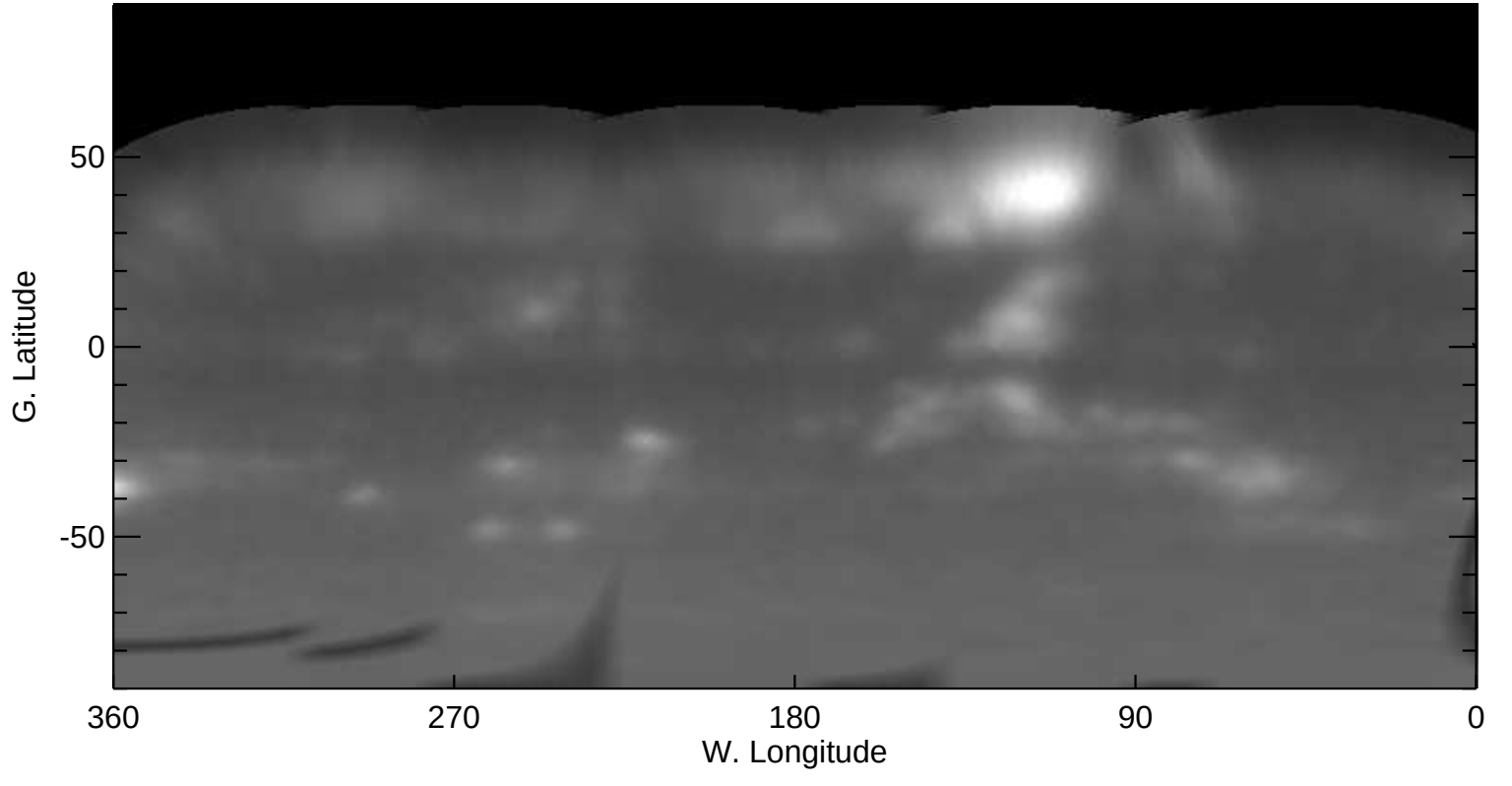
50
0
-50
G. Latitude
360
270
180
90
0
W. Longitude

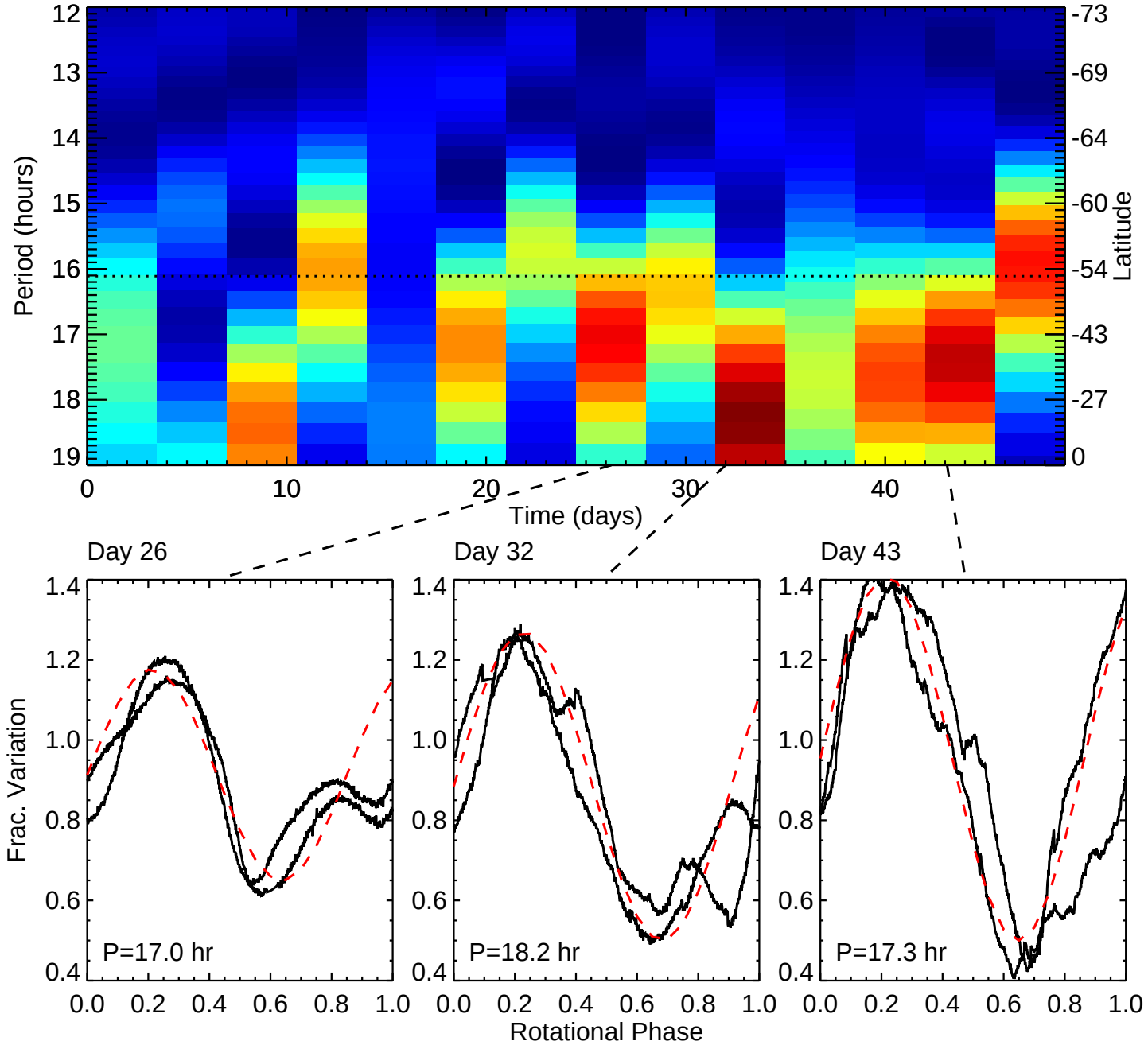
Period (hours)
12
13
14
15
16
17
18
19
-73
-69
-64
-60
-54
-43
-27
0
Latitude
0
10
20
30
40
Time (days)
Day 26
Day 32
Day 43
Frac. Variation
1.4
1.2
1.0
0.8
0.6
0.4
P=17.0 hr
P=18.2 hr
P=17.3 hr
0.0
0.2
0.4
0.6
0.8
1.0
Rotational Phase